Advances in Science and Technology Research Journal

Advances in Science and Technology Research Journal, 2026, 20(8), 38–52
https://doi.org/10.12913/22998624/220519
ISSN 2299-8624, License CC-BY 4.0

Received: 2026.02.10
Accepted: 2026.06.12
Published: 2026.07.01

Microstructural evolution and fracture behavior of Al_2O_3-Cu composites sintered without pressure

Paulina Piotrkiewicz[1], Justyna Zygmuntowicz[1*], Marcin Wachowski[2], Ireneusz Szachogłuchowicz[2], Waldemar Kaszuwara[1]

[1] Faculty of Materials Science and Engineering, Warsaw University of Technology, ul. Woloska 141, 02-507 Warsaw, Poland
[2] Faculty of Mechanical Engineering, Military University of Technology, ul. gen. S. Kaliskiego 2, 00-908 Warsaw, Poland
* Corresponding author's e-mail: justyna.zygmuntowicz@pw.edu.pl

ABSTRACT

Al_2O_3-Cu composites offer a promising combination of high hardness, thermal stability, and electrical conductivity. In this study, Al_2O_3-Cu composites containing 2.5 vol.% Cu were produced by uniaxial pressing at 100 MPa, followed by free sintering in a reducing atmosphere (95% Ar/5 % H_2). Sintering was performed at 1200 °C, 1250 °C, 1300 °C, and 1400 °C for 2 h to evaluate the influence of temperature on densification, microstructure, and mechanical properties. Phase analysis confirmed the presence of only corundum Al_2O_3 and metallic Cu, independent of sintering temperature. Relative density increased strongly with temperature, from 78.65% at 1200 °C to 96.99% at 1400 °C. Microstructural observations revealed significant copper migration at 1400 °C, leading to irregular Cu agglomerates, local depletion of the metallic phase, and the encapsulation of Al_2O_3 grains through non-wetting liquid-phase sintering. The composites sintered at 1400 °C exhibited an average hardness of 13.6 ± 1.5 GPa and an indentation fracture toughness K_{IC} of 4.94 ± 0.85 MPa·m$^{0.5}$. Fracture behavior was dominated by intergranular cracking and crack deflection at weak Al_2O_3-Cu interfaces. The results demonstrate that although high densification can be achieved without external pressure, uncontrolled copper migration remains a key limitation of pressureless sintering in Al_2O_3-Cu composites.

Keywords: Al_2O_3-Cu, composites, mechanical properties.

INTRODUCTION

Copper is a highly attractive component for ceramic matrix composites due to its high thermal and electrical conductivity, as well as its high plastic deformation capacity [1–3]. On its own, it is highly ductile, but its strength is low, which excludes its use in applications requiring strong material properties. Al_2O_3 ceramics, on the other hand, despite several advantages such as low density, high hardness, and resistance to compression and thermal shock, remain a brittle material [4–6]. The combination of these two components improves ceramic fracture resistance by introducing highly ductile metallic copper particles into the ceramic matrix [7–8]. In addition, copper, as a highly conductive component, enables the ceramic matrix composite to acquire entirely new properties, thereby expanding the material's potential for use in new applications. Research shows that adding Cu can reduce the composite's resistance compared to pure Al_2O_3 ceramics [9–10]. In turn, the rigid ceramic matrix makes the resulting Al_2O_3-Cu composite harder and more durable than pure copper. This group of composites has been admired in the scientific community for years, raising hopes for their use as components in electronic devices, sensor elements, and electromechanical applications.

The literature indicates that producing Al_2O_3-Cu composites is a complex process that entails numerous challenges. The primary technological

challenges are the low melting point of copper and its poor wettability with Al_2O_3 during sintering. This leads to difficulties in achieving a uniform distribution of copper in the ceramic matrix of the composite. This problem is exacerbated by the large difference in thermal expansion coefficients between copper and Al_2O_3, which can lead to poor adhesion between the ceramic and the metal and, consequently, the formation of voids in the composite [11]. Despite these challenges, research on the formation of composites from the Al_2O_3-Cu system continues. This research has led to the development of several methods for producing these materials. These include infiltration [12–13], slip casting [14], powder metallurgy methods [15–16] or plasma-electrolytic oxidation [17–18]. One common approach to improving wettability between liquid copper and Al_2O_3 is to introduce oxygen into the system or use cupric oxide as the starting material [19–20]. Studies have shown that the presence of oxygen reduces the contact angle in this system, facilitating bond formation between the components. This enables the production of Al_2O_3-Cu composites with a uniform distribution of the metallic phase in the matrix, resulting in good mechanical properties. The use of methods such as hot pressing and spark plasma sintering (SPS) also improved the uniform distribution of copper in the matrix, positively impacting the composite's mechanical properties [8, 13, 22]. However, despite continuous advances in knowledge related to Al_2O_3-Cu composites, achieving optimal properties remains challenging, and issues such as poor adhesion and differential shrinkage between components persist. The lack of wettability, combined with the liquid-phase sintering in Al_2O_3 composites, can lead to both an uneven distribution of the metallic phase in the matrix due to the free migration of copper during sintering and to copper flowing out of the sample. Although the available literature does not directly address copper loss, it does devote considerable attention to improving the bond between Al_2O_3 and Cu. The lack of a stable bond between copper and alumina is directly responsible for the phenomenon of copper flow. Literature data indicate that incorporating small amounts of copper (approximately 5% by volume) into the molded composite can result in satisfactory compaction and enhanced mechanical properties compared to pure Al_2O_3 [23–24]. Unfortunately, increasing the copper content often reduces material strength due to issues such as poor wettability and differences in shrinkage between components. Unfortunately, no universal solution has yet been found to optimize the properties of Al_2O_3-Cu composites produced using different methods and varying copper contents. This is a major, still unresolved technological problem that makes it difficult to control the distribution of the metallic phase in the matrix. As a result, the potential applications of these materials in areas such as electronic and electromechanical systems remain insufficiently explored.

As a result, an important gap remains in the literature: a quantitative and systematic assessment of how far pressureless sintering of Al_2O_3-Cu composites can be pushed before liquid-phase copper migration becomes the dominant microstructural failure mechanism. In particular, there is a lack of benchmark data addressing the onset and extent of copper loss and depletion during free sintering, the relationship between densification level and copper mobility, and the mechanical consequences of these effects in low-Cu-content systems, where copper particles are sparse and interfacial phenomena dominate fracture behavior.

The present study addresses this gap by providing a focused experimental investigation of Al_2O_3-Cu composites containing a low metallic phase content of 2.5 vol.% Cu fabricated by uniaxial pressing followed by pressureless sintering in a reducing atmosphere. By systematically varying the sintering temperature between 1200 °C and 1400 °C, this work quantitatively identifies a practical densification threshold approaching ~97% of theoretical density at 1400 °C, beyond which uncontrolled copper migration, agglomeration, and local depletion become pronounced. Rather than proposing a new processing solution, the study deliberately documents the limitations of pressureless sintering, demonstrating that increasing densification simultaneously intensifies liquid copper mobility and weakens the structure-property balance.

In this context, the novelty of the work lies in the quantitative demonstration of copper redistribution and loss during free sintering, the identification of a critical processing window where high density is achieved at the expense of microstructural stability, and the establishment of a reference dataset for low-Cu-content Al_2O_3-Cu composites processed without external pressure. By explicitly showing where and why pressureless sintering fails, the results provide a valuable benchmark for comparison with pressure-assisted

and chemically modified processing routes, offering guidance for future strategies aimed at stabilizing the metallic phase distribution in ceramic-metal composites.

MATERIALS AND METHODS

Commercially available α-Al_2O_3 ceramic powder, marketed under the trade name TM-DAR by Taimei Chemicals (Japan). The Cu powder (Sigma-Aldrich) used in the experiment exhibited a dendritic morphology with dendrites of varying dimensions and an average particle size of <150 μm.

Al_2O_3-Cu samples were produced by uniaxial pressing. A 10% aqueous solution of polyvinyl alcohol (PVA) was used as a binder in an amount of 10% by weight relative to the total weight of the powder mixture. The binder type and its weight percentage were selected based on previous studies conducted by the team [25–26]. The pressing process was carried out using a hydraulic press. A die made of sintered carbide with a 20 mm diameter was used to form the shapes. The pressing pressure used was 100 MPa in each case. The samples produced were characterized by a metallic phase content of 2.5% by volume. The raw shapes were then subjected to free sintering. The sintering process was carried out in a Nabertherm RHTC 80-230/16 tube furnace under a reducing atmosphere (95% Ar/5 % H_2).

The use of a reducing atmosphere was intended to prevent the formation of spinel structures and the oxidation of copper and other metallic components during sintering. Due to the low melting point of copper, which remains liquid during sintering, and the high wetting angle between pure copper and aluminum oxide, the sintering of composite samples was characterized as non-wetting liquid-phase sintering [27]. Literature studies report that the contact angle of molten copper on alumina typically exceeds 120–140° [27], confirming the strongly non-wetting character of the Cu/Al_2O_3 system. Such high contact angles significantly reduce interfacial adhesion and promote the liquid-phase mobility of copper during sintering, thereby explaining the agglomeration and migration phenomena observed in the present study. Four sintering temperatures were used: 1200 °C, 1250 °C, 1300 °C, and 1400 °C. The temperatures were selected so that the highest was the sintering temperature, enabling the production of high-density solid ceramic-metal composites on an Al_2O_3 matrix [28]. Lower temperatures were used to determine the possibility of reducing the process temperature. The sintering procedure remained the same for each sintering temperature. Heating was carried out in three stages: from 20 °C to 120 °C at 5 °C/min, from 120 °C to 750 °C at 1 °C/min, and from 750 °C to the sintering temperature at 2 °C/min. The sintering time for each temperature used was 2 hours. The system was then cooled at 4 °C/min to ambient temperature.

In this study, a copper content of 2.5 vol.% was intentionally selected as a threshold, model composition rather than as an application-optimized formulation. At such a low metallic phase fraction, copper particles are sparsely distributed within the alumina matrix and do not form a continuous or semi-continuous metallic network. As a result, the microstructural evolution and mechanical response of the composite are governed primarily by interfacial phenomena, liquid-phase mobility, and local ceramic-metal interactions, rather than by bulk metallic reinforcement effects. This compositional regime is particularly sensitive to copper migration during sintering. Even limited redistribution, agglomeration, or loss of the metallic phase leads to pronounced local depletion and heterogeneity, which can be readily detected by microstructural and mechanical analysis. Consequently, 2.5 vol.% Cu represents a critical lower-bound composition at which the intrinsic limitations of pressureless sintering, such as non-wetting liquid-phase behavior, copper coalescence, and interfacial debonding, can be isolated and quantitatively assessed without the masking effects present at higher copper contents. From a practical perspective, low copper content is also relevant for applications that require partial electrical or thermal functionality while preserving the stiffness and hardness of the ceramic matrix. However, the primary motivation of this work is not property optimization, but rather the establishment of a benchmark system for evaluating the feasibility and limits of pressureless sintering in Al_2O_3-Cu composites. The insights gained at 2.5 vol.% Cu, therefore, provide a reference framework for interpreting microstructural stability and failure mechanisms in both lower- and higher-copper-content systems processed under similar conditions.

The copper content was intentionally limited to 2.5 vol.% in order to investigate a model composite system in which the metallic phase remains

discontinuous within the ceramic matrix. Such a low volume fraction allows the study of copper mobility and redistribution during liquid-phase sintering without forming a continuous metallic network, thereby enabling analysis of interfacial phenomena characteristic of non-wetting ceramic-metal systems.

The Archimedes method was used to determine the basic physical properties of the sintered products. The measurements were carried out in accordance with PN-EN ISO 18754:2022-10 [29]. To determine the individual parameters, the mass of the samples was measured in their initial state in air. Afterward, they were soaked in an immersion liquid, and their mass was measured again in both air and water. Demineralized water was used as the immersion liquid. Based on the measurements, the relative density, soaking, and open porosity of the samples were determined.

Sintered composite samples were subjected to phase composition analysis. All measurements were performed on a Rigaku Miniflex II powder diffractometer using a copper lamp with a wavelength of 1.54059 Å, an output voltage of 30 kV, and a current of 15 mA. The angular range of the measurements was 20–100° of the 2Θ angle, with a shift of 0.01° and a counting time of 1 s. The analysis of the diffraction patterns obtained from the tests was performed using the PDF+4 2022 reference database and the correlated Jade 8.5 program (Materials Data).

The surfaces of the sintered products were examined using an Olympus LEXT OLS4100 confocal microscope in order to make a general assessment of the distribution of the metallic phase in the composite structure.

The surfaces of sintered composite shapes and their fractures were observed using a Jeol JSM-6610 scanning electron microscope. The observations were conducted in both backscattered electron (BSE) and secondary elastic scattering (SE) modes at an accelerating voltage of 15 kV. The samples intended for observation were previously coated with a thin layer of carbon using a JEOL Finecoat Ion Sputter JFC-1100.

In this study, phase composition was analyzed using a JEOL JSM-6610 scanning electron microscope equipped with an energy-dispersive X-ray detector. During observation, maps of element distribution in selected areas of the samples were prepared, accounting for connections at the boundary between the ceramic matrix and the metallic components.

Hardness measurements were performed on flat parallel surfaces of sintered samples from all series after metallographic preparation. The test was conducted using an HVS-30T hardness tester manufactured by Huatec Group Corporation. For all measurements, an identical load of 98 N was applied for 15 seconds.

The fracture toughness of the investigated composites was estimated using the indentation fracture method based on Vickers indentation. It should be noted that indentation-derived fracture toughness values provide only approximate estimates of the resistance to crack propagation, particularly in heterogeneous materials such as ceramic-metal composites. The method is sensitive to several factors, including crack morphology, residual stresses, and microstructural heterogeneity, which may influence the accuracy of the calculated values. Therefore, the obtained results should be interpreted primarily in a comparative manner when evaluating the influence of sintering temperature on fracture resistance. For a more rigorous determination of macroscopic fracture toughness, standardized fracture mechanics methods such as the single-edge notched beam (SENB) or chevron-notched beam (CNB) techniques are generally recommended, as they provide more reliable and reproducible measurements of fracture parameters in brittle materials. In the present study, the fracture toughness values were calculated using the relationship proposed by Lankford [30] for radial-median cracks generated during Vickers indentation. This approach allows for a consistent comparison of fracture resistance among samples processed under different sintering conditions.

The mechanical behavior of the fabricated Al_2O_3-Cu composites after sintering was systematically evaluated using uniaxial compression testing, with the dual objectives of quantifying compressive strength and elucidating the deformation and fracture mechanisms governing failure. Given the heterogeneous nature of ceramic-metal composites, particular emphasis was placed on correlating the macroscopic mechanical response with local strain evolution and damage initiation. Uniaxial compression tests were performed using a servo-hydraulic testing system (Instron 8802 MT) operating under displacement-controlled conditions, which ensured stable loading and precise control over the deformation rate. The system was equipped with a high-accuracy load cell and integrated with dedicated control and

data-acquisition software, enabling continuous, synchronous recording of applied force and crosshead displacement throughout the entire loading cycle. The displacement-controlled regime was selected to minimize dynamic instabilities and to allow detailed observation of pre-failure deformation behavior, which is particularly critical for quasi-brittle materials such as ceramic-based composites. Prior to testing, all specimens were carefully prepared to ensure parallelism and planarity of the loading surfaces, thereby minimizing stress concentrations and preventing premature failure from misalignment. During testing, the samples were positioned centrally between hardened steel compression platens, with special attention paid to axial alignment to promote uniform load transfer and reduce bending stresses. This step is essential for obtaining reliable compressive-strength values, especially in materials with limited plastic deformation capacity. The compressive load was applied monotonically at a constant displacement rate until catastrophic failure occurred. The failure point was defined as the maximum stress corresponding to the first pronounced drop in the load-displacement curve, which is indicative of rapid crack propagation and loss of load-bearing capacity. In all cases, failure was accompanied by the formation of a macroscopically visible fracture, typically characterized by axial splitting and shear localization, consistent with the brittle or quasi-brittle nature of the investigated composites. To complement the conventional mechanical measurements, the deformation behavior of the specimens was analyzed using a non-contact, full-field optical technique based on Digital Image Correlation (DIC). This approach enables spatially resolved measurement of displacement and strain fields across the specimen surface, providing critical insight into strain localization, damage initiation, and crack propagation mechanisms that cannot be captured by global measurements alone. The DIC measurements were performed using a Dantec Dynamics Q400 system, equipped with two synchronized high-resolution cameras (8 MP each) in a stereoscopic setup. This configuration enables three-dimensional displacement field reconstruction, ensuring accurate strain quantification even in the presence of out-of-plane motion. Prior to testing, the specimen surfaces were prepared with a stochastic speckle pattern to facilitate reliable image correlation. The system provided a displacement measurement accuracy of ±0.01 pixels, corresponding to a strain resolution of approximately 0.01%, enabling the detection of even subtle deformation heterogeneities. Image acquisition, correlation, and post-processing were performed using the ISTRA 4D software suite, which enabled the generation of high-resolution strain maps throughout the loading process. These full-field strain distributions were used to identify regions of strain concentration, which are typically associated with microstructural heterogeneities such as copper agglomerates, interfacial debonding zones, or residual porosity. The evolution of these localized strain fields provided direct evidence of damage initiation sites and allowed for a detailed analysis of the transition from distributed deformation to localized failure. All tests were conducted under controlled laboratory conditions at 22 ± 2 °C to eliminate environmental variability. A total of eight specimens per material series were tested to ensure statistical reliability and reproducibility of the results. The reported mechanical properties, including compressive strength, were calculated as average values, and the corresponding variability was assessed to account for inherent microstructural heterogeneity. The results presented in the subsequent section include representative force-displacement curves that characterize the global mechanical response, as well as corresponding strain field maps from DIC analysis, which illustrate the spatial distribution and evolution of deformation leading up to failure. This combined experimental approach enables a comprehensive understanding of the interplay between microstructure and mechanical performance in Al_2O_3-Cu composites, particularly regarding strain localization, interfacial effects, and fracture mechanisms.

The quantitative characterization of the Al_2O_3 matrix grain size was performed using a stereological approach, ensuring statistically reliable and reproducible results. Fracture surfaces of the sintered samples were examined by scanning electron microscopy (SEM), which enabled high-resolution observation of the ceramic microstructure without additional surface preparation that could alter grain boundaries. To achieve robust statistical representation, 15 SEM micrographs per sample were acquired for each of the five specimens sintered at 1400 °C. All images were collected at identical magnification and resolution, and the observation fields were selected randomly across the fracture surface to eliminate operator bias and account for possible microstructural heterogeneity. Prior to

image analysis, each micrograph was carefully calibrated using the SEM scale bar to ensure dimensional accuracy. Grain identification was performed using a semi-manual detection procedure, in which individual Al_2O_3 grains were delineated while accounting for the three-dimensional microstructure projected onto a two-dimensional plane. Subsequently, a sequence of image processing operations, including contrast enhancement, filtering, and thresholding, was applied to extract grain boundaries and generate binary images suitable for quantitative analysis. The processed images were analyzed using Micrometer software [31–34], which enabled precise determination of stereological parameters. In total, more than 3000 individual grains per sample were measured, a number widely recognized in stereological practice as sufficient to ensure statistical confidence and minimize sampling error. The large dataset significantly reduces uncertainty associated with local variations in grain size distribution. Grain size was quantified using the equivalent circle diameter (d_2), defined as the diameter of a circle having the same projected area as the measured grain. This parameter provides a standardized means of describing irregular, non-spherical particles and is commonly used in microstructural analysis [35]. The equivalent diameter was calculated directly from the measured grain area for each detected particle. The results were statistically processed and are reported as mean grain size (d_2) ± standard deviation, derived from the full population of measured grains. Additionally, the grain size distributions were presented in the form of percentage-based histograms, allowing detailed assessment of microstructural uniformity and the presence of any abnormal grain growth. The combination of a sufficiently large number of analyzed micrographs, random field selection, and a high number of measured grains ensures that the obtained grain size distributions are representative of the bulk material. Consequently, the applied methodology provides a reliable and statistically robust description of the Al_2O_3 matrix microstructure, meeting the requirements for rigorous quantitative analysis.

RESULTS AND DISCUSSION

In the first stage of the research, it was decided to test the phase composition of the produced shapes after sintering. It was found that the Al_2O_3-Cu composites produced by uniaxial pressing after sintering were characterized by the presence of two phases: Al_2O_3 in the form of corundum (PDF #98-000-0174) and Cu (PDF #04-013-9963). Analysis of the diffraction patterns obtained for the samples revealed no effect of sintering temperature on the

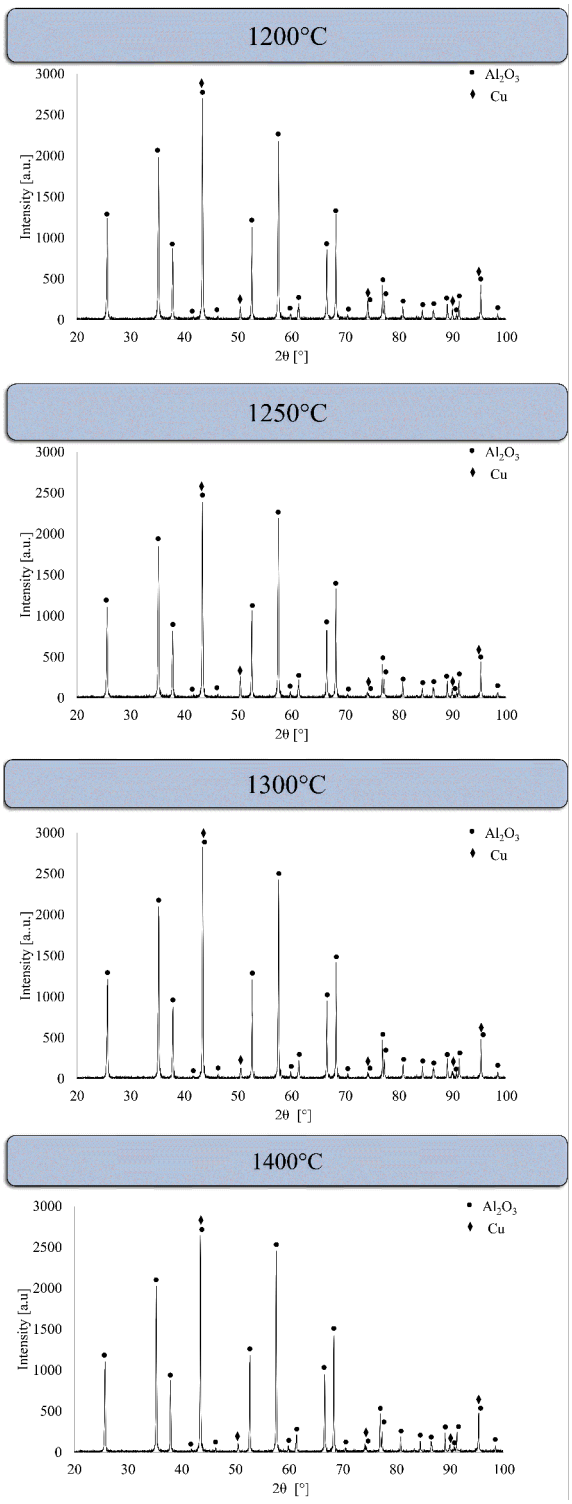

Figure 1. X-ray diffraction (XRD) patterns of Al_2O_3-Cu composites containing 2.5 vol.% Cu sintered at different temperatures (1200–1400 °C) in a reducing atmosphere (95% Ar / 5% H_2)

phase composition. No effect of the sintering temperature of Al_2O_3-Cu composites on the appearance of new phases was observed.

Analysis of the shapes formed by uniaxial pressing clearly indicates a relationship between sintering temperature and the relative density of the resulting sinters. The relative density of the samples increased visibly with increasing sintering temperature. The lowest relative density was obtained for samples sintered at 1200 °C, for which it was 78.65 ± 0.97 % of theoretical density. The highest relative density, 96.99 ± 0.94% of the theoretical density, was obtained during sintering at 1400 °C. The relative densities of samples sintered at 1250 °C and 1300 °C were 85.42 ± 1.23% and 89.68 ± 1.03%, respectively. In the case of uniaxial pressing with free sintering, no additional pressure is applied, which could aid copper migration and reduce pores, especially at the lower sintering temperatures used in the experiment.

As a consequence, a clear dependence of the obtained densification on the sintering temperature may be visible in these samples. Samples sintered at 1200 °C exhibited high open porosity of 20.57 ± 0.67% and a corresponding water absorption of 5.97 ± 0.46%, indicating limited densification and modest volumetric contraction. Increasing the sintering temperature to 1250 °C resulted in a marked decrease in open porosity to 13.95 ± 0.73% and water absorption to 3.82 ± 0.12%, indicating enhanced shrinkage associated with improved particle rearrangement and neck growth. Further densification occurred at 1300 °C, where the open porosity was reduced to 9.39 ± 0.72% and water absorption to 2.49 ± 0.07%. At the highest sintering temperature of 1400 °C, near complete densification was achieved, with open porosity decreasing to 0.11 ± 0.07% and water absorption to 0.02 ± 0.05%. This reduction in accessible pore volume indicates substantial volumetric shrinkage, driven by intensified mass transport and liquid-phase-assisted densification induced by molten copper. The results confirm that increasing sintering temperature promotes volumetric contraction of the composite body. However, at elevated temperatures, this process coincides with increased copper mobility, which compromises microstructural stability despite the high degree of densification.

The results indicate a critical processing window near 1400 °C, where relative density approaches ~97%, but microstructural stability deteriorates due to increased copper mobility. This behavior reflects a fundamental limitation of liquid-phase sintering in non-wetting systems, where densification and phase stability compete. Moreover, in this regime, the formation of a transient liquid copper phase enhances densification while simultaneously promoting phase separation and redistribution.

The volumetric shrinkage of the Al_2O_3-Cu composites can be inferred from the systematic reduction in open porosity and water absorption with increasing sintering temperature. Moreover, the volumetric shrinkage of the Al_2O_3-Cu composites showed a strong dependence on sintering temperature, reflecting the material's progressive densification. Samples sintered at 1200 °C showed a volumetric shrinkage of 23.27 ± 0.87%, which increased to 29.91 ± 0.85% at 1250 °C and 34.95 ± 0.75% at 1300 °C. The highest shrinkage, reaching 40.91 ± 0.62%, was recorded for samples sintered at 1400 °C. This monotonic increase in volumetric shrinkage is consistent with enhanced mass transport and pore elimination at elevated temperatures. At lower sintering temperatures, shrinkage is primarily governed by solid-state diffusion within the alumina matrix, resulting in limited densification.

In contrast, at 1400 °C, the presence of liquid copper significantly accelerates densification through the liquid-phase-assisted rearrangement of ceramic particles, resulting in a substantial volume reduction. However, this intensified shrinkage is accompanied by increased copper mobility, which contributes to the migration of the metallic phase and local depletion. Therefore, while higher sintering temperatures promote densification and volumetric shrinkage, they simultaneously exacerbate microstructural instability associated with non-wetting liquid-phase sintering of copper.

The primary objective of the present study was to investigate the microstructural evolution and mechanical consequences of pressureless sintering in a poorly wetting ceramic-metal system, rather than to determine the exact compositional balance after sintering. In the conducted research, the observed copper redistribution is inferred from microstructural evidence, such as copper agglomeration and the formation of local copper-depleted regions, rather than from direct compositional measurements.

Since samples sintered at 1400 °C were included in further research due to their properties, it was decided to present only these shapes after sintering. Example photos of composite

samples of the reference series Al_2O_3-Cu with 2.5% vol. metallic phase content are shown in Figure 2. Macroscopic observations of the produced samples revealed the absence of surface defects resulting from uniaxial pressing with free sintering at 1400 °C.

Figure 3 presents sample surface observation results for composite samples with a 2.5% metallic phase content produced by uniaxial pressing with free sintering. Observations were performed using a confocal microscope. Surface analysis of the Al_2O_3-Cu samples revealed that metallic particles in the matrix were randomly distributed. In the sample produced by uniaxial pressing and then free-form sintered at 1400 °C (Figure 3), a depletion of the metallic phase was observed in the central area. This may be due to copper loss from the sample's surface layers during sintering. The presence of metallic particles of varying sizes characterizes the sample. Copper particles, which are in a liquid state during free sintering, coalesce upon contact into larger clusters before being enclosed by the growing matrix particles. The long duration of the process promotes both the flow of copper beyond the sample surface and the formation of areas with varying particle sizes and metallic phase content.

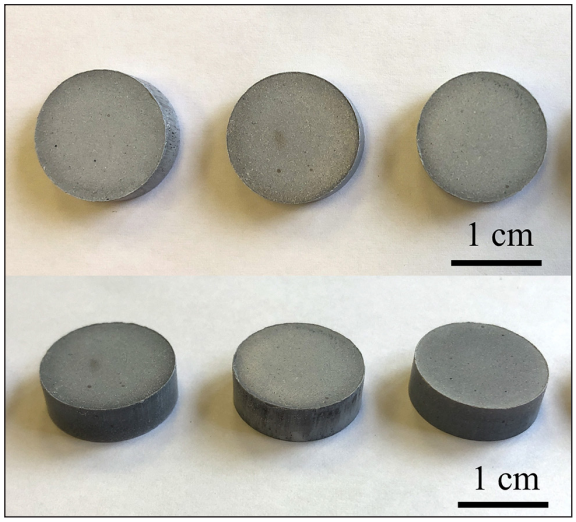

Figure 2. Macroscopic appearance of Al_2O_3-Cu composite with 2.5% vol. metallic phase content after forming using uniaxial pressing, after free sintering in a reducing atmosphere at temperatures of 1400 °C for 2 h

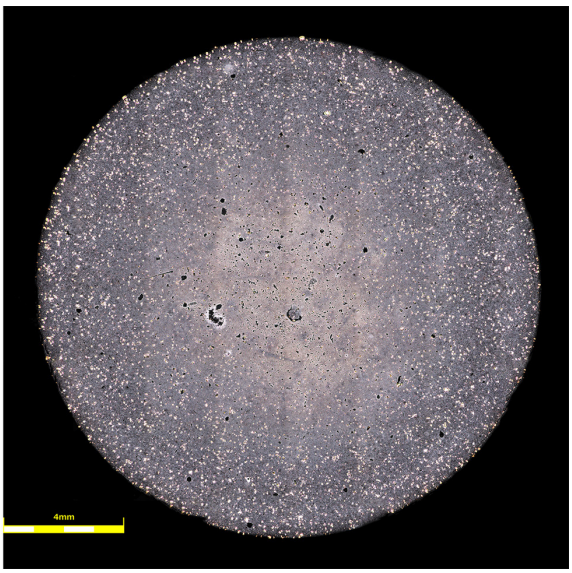

Figure 3. Example micrographs of the surface of samples from the Al_2O_3-Cu system with 2.5% vol. metallic phase content after sintering at 1400 °C

In the next step, SEM observations were performed on composite samples from Al_2O_3-Cu systems, uniaxially pressed and freely sintered at 1400 °C (Figure 4), which revealed irregularly shaped metallic particles of varying sizes within the ceramic matrix. It was found that within the observed metallic particles, both near the outer edge and in the central part, there were enclosed single matrix particles. Due to its low melting point (1083 °C [36]), copper remains liquid during sintering. Poor wettability between metallic copper and the ceramic Al_2O_3 matrix contributes to Cu migration within the sample during sintering. Migrating copper encounters other metallic particles and combines with them, forming metallic phase agglomerates observed in the microstructure. During this process, the matrix particles, originally located between separate copper particles, become encapsulated within the developing agglomerates. Subsequently, when the matrix sintering occurs after reaching a predetermined temperature, the Al_2O_3 particles coalesce, preventing further migration of the liquid copper. This results in the formation of the observed copper agglomerates with an irregular metal-ceramic interface, with the Al_2O_3 particles encapsulated within.

EDS analysis was performed with a focus on the metallic particles in the matrix, accounting for their interactions with the matrix and the area immediately adjacent to each particle. The results were presented as mappings showing the share of individual elements in selected areas of the microstructure (Figure 5). The analysis revealed the presence of three elements in the indicated fragment of the microstructure: Al, O, and Cu. The presence of copper was limited to the

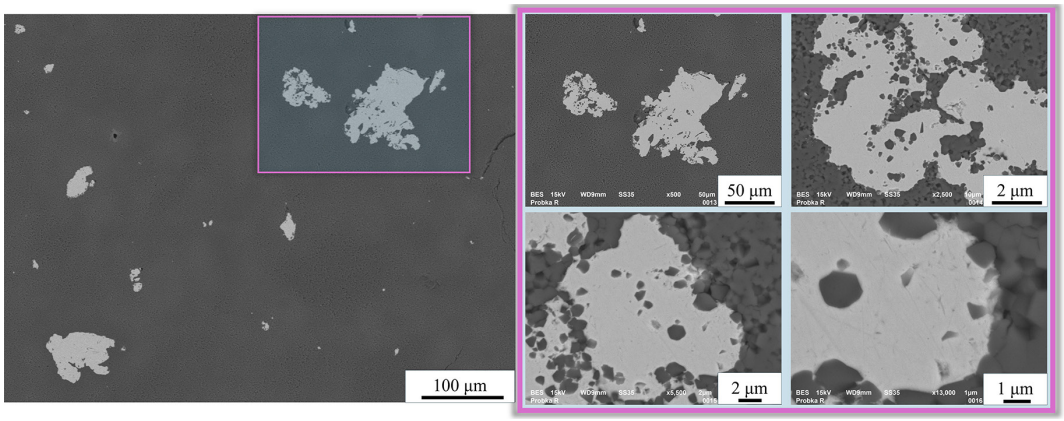

Figure 4. Representative scanning electron microscopy (SEM) micrographs of the microstructure of Al_2O_3-Cu composites containing 2.5 vol.% Cu sintered at temperatures of 1400 °C. Images recorded in backscattered electron (BSE) mode highlight the contrast between the ceramic matrix (Al_2O_3, darker) and the metallic phase (Cu, brighter)

metallic particle area, while both aluminum and oxygen were present in the remaining portion of the microstructure corresponding to the matrix. A visible demarcation between the metallic particle and the matrix characterized the areas of element occurrence in the microstructure.

Mechanical tests were then conducted. Mechanical testing was limited to the highest-density samples to avoid results dominated by porosity. The series sintered at lower temperatures (1200 °C, 1250 °C, 1300 °C) was excluded from the study due to unsatisfactory densification, determined to be below 90% of the theoretical density. Analysis of the results for the Al_2O_3-Cu samples showed that the pressed samples sintered at 1400 °C had an average hardness of 13.6 ± 1.5 GPa. Based on the literature, the results obtained for the produced ceramic-metal composites differ from those for the Al_2O_3 ceramic samples. In studies on Al2O3 ceramic samples prepared by the PPS method using the same commercial ceramic powder (Al2O3 TM-DAR) and identical process parameters, the samples' hardness increased with increasing temperature. The measured values for samples formed at 1200 °C, 1300 °C, and 1400 °C were 18.30 ± 0.50 GPa, 19.20 ± 0.54 GPa, and 21.00 ± 0.60 GPa [37], respectively. Similar results were obtained in studies that used another current sintering method for Al_2O_3 [38]. An experiment conducted by S. Huang's team

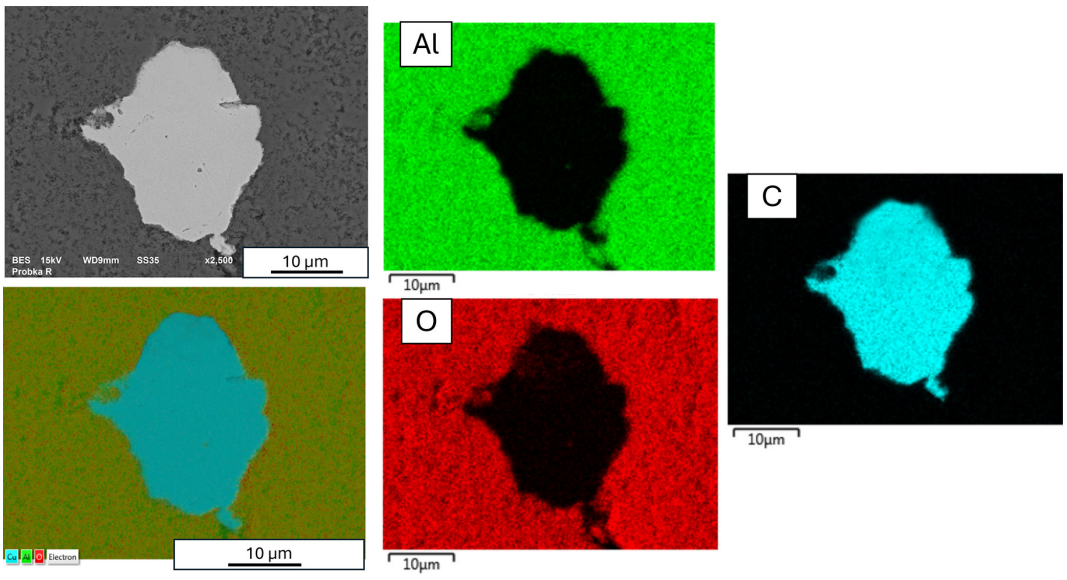

Figure 5. SEM image and corresponding energy-dispersive X-ray spectroscopy (EDS) elemental analysis of an Al_2O_3-Cu sample with 2.5% vol. metallic phase content produced by uniaxial pressing and sintered at 1400 °C

showed that the hardness of ceramic samples formed from Al_2O_3 TM-DAR powder at 1250 °C was 20.0 ± 0.5 GPa, while at 1450 °C it was 19.4 ± 0.4 GPa [38]. The process was carried out at a densification pressure of 60 MPa, which was applied to the sample during its holding time at the maximum temperature. Thanks to the applied process parameters, densification of both samples was achieved close to 100% [38].

For Al2O3-Cu samples, the KIC value for a sample produced by uniaxial pressing and sintered at 1400 °C was 4.94 ± 0.85 MPa $m^{0.5}$. In these samples, the probability of a crack encountering a metallic particle is low. However, given the weak adhesion between the metallic phase and the ceramic matrix, the only mechanism observed in the samples is crack deflection. Cracks propagated along the lowest-energy path at the interface between the components. Metallic particles cannot completely stop the material from cracking; they only extend the crack propagation path and, therefore, the time from crack initiation to sample failure. It should be emphasized that the fracture toughness values reported in this study, determined using the indentation method, should be interpreted as upper-bound estimates rather than intrinsic material constants. Owing to the pronounced microstructural heterogeneity of the Al_2O_3-Cu composites stemming from non-uniform copper distribution, agglomeration of the metallic phase, and local porosity, the probability of crack interaction with copper particles varies significantly from indentation to indentation. In regions where cracks intersect metallic agglomerates or propagate along extended ceramic-metal interfaces, enhanced crack deflection may artificially increase the apparent K_{IC} value. Conversely, crack propagation through copper-depleted or highly porous regions is not adequately captured by localized indentation measurements.

Furthermore, indentation-based fracture toughness methods are known to be sensitive to residual stresses, elastic-plastic mismatch between phases, and the choice of analytical relationship used for K_{IC} estimation. In heterogeneous ceramic-metal composites, these factors may collectively lead to an overestimation of the effective fracture resistance of the bulk material. Therefore, the K_{IC} values reported here should be regarded as an upper-limit indication of local crack-growth resistance, reflecting favorable crack microstructure interactions rather than the macroscopic fracture toughness that would be obtained from standardized fracture mechanics tests. The method for determining material fracture toughness using cracks extending from the indenter corners is commonly used for ceramic samples and ceramic-based composites [39-41]. This group of methods allows fracture toughness analysis directly on prepared samples, without the need to fabricate additional shapes with a given geometry, which is complicated for ceramic materials due to their properties. Given the heterogeneity of the metallic phase distribution in ceramic-metal composites, this can lead to results with significant errors [41]. However, it should be noted that the values obtained using the indenter method also depend on many factors, including the equation used to determine the critical stress intensity factor.

The strain distribution during the loading process for Al_2O_3-Cu samples with a 2.5% metallic phase content is shown in Figure 6. The material exhibits a continuous increase in load from the beginning of the test; however, the peak region is marked by a sudden drop in force, indicating abrupt crack propagation and a damage event during compression. The loading response prior to failure is predominantly elastic and characterized by a linear increase in force with increasing displacement, reflecting a gradual increase in material stiffness throughout the test. At small displacements (up to approximately 0.6 mm), the load increases slowly, suggesting initial compliance of the composite. This behavior may be related to elastic deformation, microstructural rearrangements, or settling effects within the testing system. Beyond this stage, the curve becomes steeper, indicating a significant increase in stiffness and a more effective load-bearing response. In the approximately 0.6-0.8 mm displacement range, the force rises rapidly, corresponding to the dominant deformation regime in which the material strongly resists further displacement. At larger displacements (above approximately 0.8 mm), the rate of force increase gradually diminishes, which may indicate the onset of damage accumulation, material saturation, or nonlinear plastic behavior. The maximum recorded load is approximately 13 kN. The determined value of compressive strength for Al_2O_3-Cu shapes was 63.42 ± 0.95 MPa. This mechanical response suggests a relatively violent damage evolution and a transition from distributed microcracking to macroscopic fracture. The shape of the load-displacement curve provides insight into the prevailing fracture mechanisms. The composite behaves

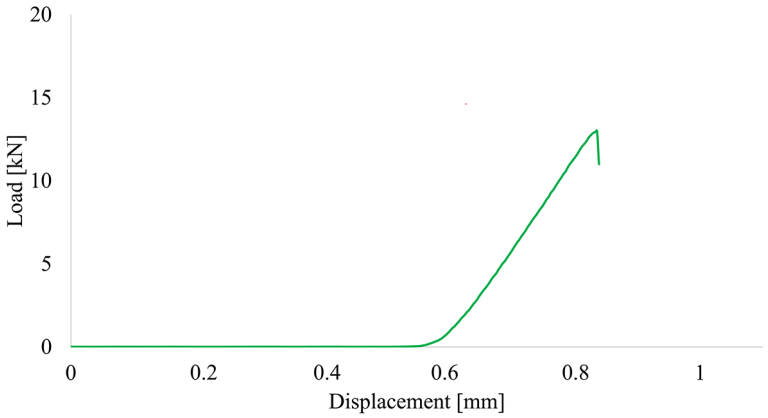

Figure 6. Load-displacement curves obtained during uniaxial compression testing of Al_2O_3-Cu system composites containing 2.5 vol.% Cu

elastically up to crack initiation, without a distinct plastic plateau.

Once the maximum load is reached, failure occurs rapidly. The serrated character of the curve indicates a fracture process governed by localized damage events. Copper particles may act as stress concentrators due to their non-uniform distribution within the ceramic matrix. During compression, crack initiation is likely to occur preferentially at ceramic-metal interfaces or in regions containing clustered or weakly bonded Cu particles. The stepwise drops in load reflect the successive coalescence of microcracks and the intermittent formation of dominant shear cracks, which together govern the composite's overall compressive response.

An example of the strain distribution during loading of samples from the Al_2O_3-Cu produced by uniaxial pressing with free sintering at 1400 °C is shown in Figure 7. In the sinter produced by conventional sintering at 1400 °C, the action of monotonic loading accentuated strain concentrations. These were located at the contact points between the sample and the punches, i.e., at the highest unit pressures. The material exhibited low susceptibility to deformation, with fracture occurring on both sides of the vertical axis.

By analyzing the mechanical results, it can be concluded that, first, the inherently poor wettability of the Al_2O_3/Cu system (contact angle ~120–140°) leads to weak interfacial bonding, significantly reducing load transfer efficiency between the metallic and ceramic phases. Second, copper agglomeration during sintering results in the formation of discrete metallic clusters that act as stress concentrators, facilitating crack initiation under compressive loading. Third, the presence of copper-depleted regions results in locally unreinforced ceramic zones, thereby reducing the effectiveness of crack-bridging and crack-deflection mechanisms. Additionally, the non-uniform spatial distribution of copper introduces microstructural heterogeneity, resulting in localized stress gradients and premature failure. These results demonstrate that near-full densification does not guarantee high mechanical strength in non-wetting

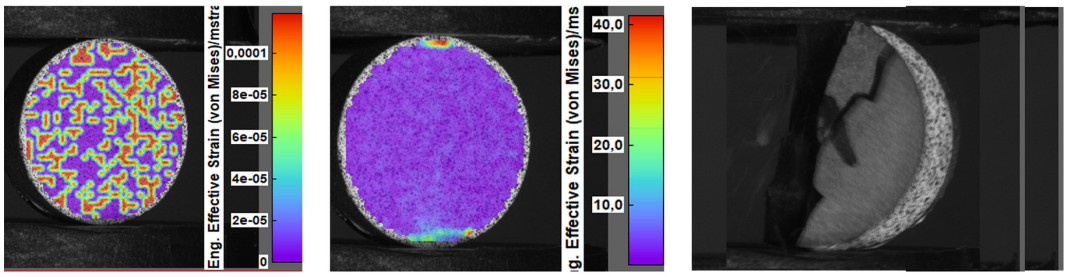

Figure 7. Example strain distribution maps obtained by digital image correlation (DIC) during compressive loading of an Al_2O_3-Cu system with 2.5% vol. metallic phase content produced by uniaxial pressing with free sintering at 1400 °C. The maps illustrate the evolution of local strain fields and the initiation of deformation localization prior to fracture

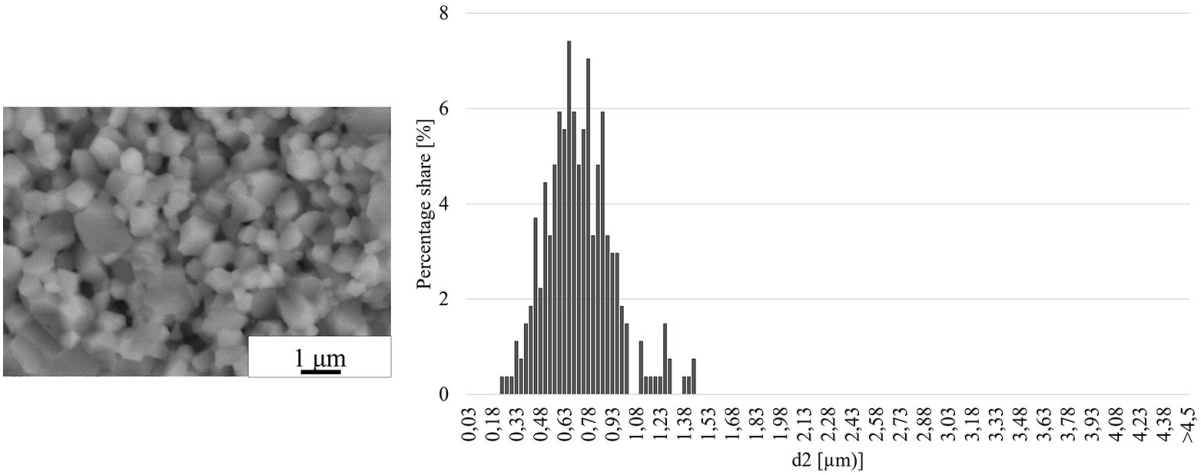

Figure 8. Representative fracture surface micrograph of an Al_2O_3-Cu composite after compressive failure together with alumina grain size analysis

ceramic-metal systems, where interfacial integrity and phase distribution are dominant factors in determining mechanical performance.

Next, the results of fracture observations of composite samples formed after compressive strength testing are presented, along with the percentage distribution of Al_2O_3 particle sizes. The matrix particle size was determined by image analysis of SEM images of the fractures. The low melting point of Cu prevented thermal etching without interfering with the composite microstructure. Therefore, manual detection of Al_2O_3 grains was performed for each of the tested samples. Image analysis was used to determine the sinter's mean equivalent diameter (d_2). The mean equivalent diameter d_2 defines the diameter of a circle with a surface area corresponding to the surface area of the analyzed particle [35].

Analysis of the results obtained for samples from the Al_2O_3-Cu system (Figure 8) showed that the mean equivalent diameter of Al_2O_3 particles for the sample produced by conventional sintering was 0.71 ± 0.22 µm. Fractographic observations revealed numerous large pores between the matrix particles in this sample. The fracture nature indicates that the sample fractured intergranularly, with the crack propagating along grain boundaries.

CONCLUSIONS

This study addresses a long-standing technological challenge in ceramic-metal composites: how to process alumina-copper materials when copper does not wet alumina and becomes liquid during sintering. These issues often lead to copper migration, loss of metallic phase, porosity, and weak ceramic-metal bonding, which limit mechanical performance and practical applicability. This work investigates the relationships between processing microstructure and properties of Al_2O_3-Cu ceramic-metal composites fabricated by uniaxial pressing and pressureless sintering, with a focus on the challenges associated with non-wetting liquid-phase sintering of copper. Composites containing 2.5 vol.% Cu were pressed at 100 MPa and sintered for 2 h in a reducing atmosphere (95% Ar / 5% H_2) at temperatures ranging from 1200 °C to 1400 °C. X-ray diffraction confirmed a stable two-phase system consisting exclusively of corundum Al_2O_3 and metallic Cu, with no secondary phases formed over the investigated temperature range.

Densification was strongly temperature-dependent, increasing from 78.65 ± 0.97% of theoretical density at 1200 °C to 96.99 ± 0.94% at 1400 °C. Microstructural analyses revealed that, at 1400 °C, copper remained liquid during sintering and exhibited pronounced migration, coalescence, and partial outflow from the sample, resulting in irregular Cu agglomerates, local depletion of the metallic phase, and encapsulation of Al_2O_3 grains. The average equivalent diameter of Al_2O_3 grains in the matrix was 0.71 ± 0.22 µm, and fracture surfaces indicated predominantly intergranular failure with significant porosity.

Mechanically, the composites sintered at 1400 °C exhibited a Vickers hardness of 13.6 ± 1.5 GPa and an indentation fracture toughness K_{IC} of 4.94 ± 0.85 MPa·$m^{0.5}$. Toughening was

governed mainly by crack deflection along weak Al_2O_3-Cu interfaces rather than by effective crack bridging. The study demonstrates that while near-full densification can be achieved without external pressure, uncontrolled copper migration remains a critical limitation, restricting further improvements in the mechanical performance of pressureless sintered Al_2O_3-Cu composites. The determined value of compressive strength for Al_2O_3-Cu shapes was 63.42 ± 0.95 MPa. It should be noted that the redistribution of copper observed in this study is inferred from microstructural observations and elemental mapping rather than from direct quantitative compositional measurements. Although copper agglomeration and local depletion zones are clearly visible in the microstructure, precise quantification of copper loss would require complementary analytical techniques, such as ICP-OES, XRF, or quantitative image analysis of the metallic phase fraction. Such measurements will be addressed in future work.

By explicitly linking processing conditions, copper mobility, microstructure evolution, and mechanical response, the study provides valuable insight into the limitations of pressureless sintering for Al_2O_3-Cu composites. Importantly, it highlights that even small copper additions can alter fracture behavior. However, poor wettability and liquid-phase migration remain the dominant obstacles to property optimization.

Acknowledgment

This work was financed/co-financed by the Military University of Technology under research project 531-000104-W100-22.

REFERENCES

1. Yan Y.-F., Kou S.-Q., Yang H.-Y., Shu S.-L., Qiu F., Jiang Q.-C., Zhang L.-C. Ceramic particles reinforced copper matrix composites manufactured by advanced powder metallurgy: preparation, performance, and mechanisms. International Journal of Extreme Manufacturing 2023; 5(3): 035001. https://doi.org/10.1088/2631-7990/acdb0b
2. Kunčická L., Walek J., Kocich R. Microstructure development of powder-based Cu composite during high shear strain processing. Metals 2024; 14(12): 1331. https://doi.org/10.3390/met14121331
3. Zhong S., Zhang X., Liu A., Zhang B. Electrical and thermal conductivity of graphene/copper composites and their applications in high-efficiency current-carrying conductors: A review. Advanced Engineering Materials 2025; 27: 2401950. https://doi.org/10.1002/adem.202401950
4. Tanwar R.S., Sarkar S., Vignesh M., Jhavar S. Additive manufacturing of Al_2O_3 ceramic components: Rheological and microstructural characterization. In: Bhingole P., Joshi K., Yadav S.D., Sharma A., editors. Advances in Materials Engineering. Lecture Notes in Mechanical Engineering. Springer 2025. https://doi.org/10.1007/978-981-97-7114-1_11
5. Chen X., Jiang Y., Sun X., Jiang R., Liu H. Micro- and macro-mechanical properties of an Al_2O_3/Al_2O_3 ceramic matrix composite after thermal aging at 1400 °C. Materials Today Communications 2024; 40: 109747. https://doi.org/10.1016/j.mtcomm.2024.109747
6. Rubino F., Rotella G., Perrella M., et al. Microstructural and mechanical properties of Al_2O_3 and Al_2O_3/TiB_2 ceramics consolidated by plasma pressure compaction. Journal of Materials Engineering and Performance 2023; 32: 4391–4403. https://doi.org/10.1007/s11665-022-07403-1
7. Hussain M.Z., Khan U., Jangid R., Khan S. Hardness and wear analysis of Cu/Al_2O_3 composite for application in EDM electrode. IOP Conference Series: Materials Science and Engineering 2018; 310: 012044. https://doi.org/10.1088/1757-899X/310/1/012044
8. Chen Y., Ud-din R., Yang T., Li T., Li C., Chu A., Zhao Y. Preparing and wear-resisting property of Al_2O_3/Cu composite material enhanced using novel in situ generated Al_2O_3 nanoparticles. Materials 2023; 16(13): 4819. https://doi.org/10.3390/ma16134819
9. Shi Z., Yan M. The preparation of Al_2O_3–Cu composite by internal oxidation. Applied Surface Science 1998; 134(1–4): 103–106. https://doi.org/10.1016/S0169-4332(98)00223-2
10. Rajkovic V., Bozic D., Jovanovic M.T. Effects of copper and Al_2O_3 particles on characteristics of Cu- Al_2O_3 composites. Materials & Design 2010; 31(4): 1962–1970. https://doi.org/10.1016/j.matdes.2009.10.037
11. Li Y., Wang J., Shen Z., et al. Application of Ag-Cu-Ti active metal composite filler in ceramic joining: A review. Frontiers in Materials Science 2023; 17: 230664. https://doi.org/10.1007/s11706-023-0664-6
12. Pfeiffer S., Lorenz H., Fu Z., Fey T., Greil P., Travitzky N. Al_2O_3/Cu-O composites fabricated by pressureless infiltration of paper-derived Al2O3 porous preforms. Ceramics International 2018; 44(17): 20835–20840. https://doi.org/10.1016/j.ceramint.2018.08.087
13. Shi Y., Chen W., Dong L., Li H., Fu Y. Enhancing

copper infiltration into alumina using spark plasma sintering to achieve high performance Al_2O_3/Cu composites. Ceramics International 2018; 44(1): 57–64. https://doi.org/10.1016/j.ceramint.2017.09.062

14. Wachowski M., Kaszuwara W., Miazga A., Konopka K., Zygmuntowicz J. The possibility of producing graded Al_2O_3-Mo, Al_2O_3-Cu, Al_2O_3-W composites using CSC method. Bulletin of the Polish Academy of Sciences: Technical Sciences 2019; 67(2). https://doi.org/10.24425/bpas.2019.128603
15. Meilakh A.G., Kontsevoy Y.V., Shubin A.B., et al. Activated sintering of Cu-Al_2O_3 powders. Inorganic Materials: Applied Research 2018; 9: 490–497. https://doi.org/10.1134/S2075113318030218
16. Yang T., Chu A., Li T., Zhao Y., Dong Z., Guo S. Preparation of Al_2O_3/Cu porous composites by combination of solution combustion synthesis and powder metallurgy method. Fenmo Yejin Jishu 2023; 43(2): 206–214. https://doi.org/10.19591/j.cnki.cn11-1974/tf.2023100012
17. Hutsaylyuk V., Student M., Posuvailo V., Student O., V., Maruschak P., Zakiev V.. The role of hydrogen in the formation of oxide-ceramic layers on aluminum alloys during their plasma-electrolytic oxidation, Journal of Materials Research and Technology, 2021; 14: 1682-1696, https://doi.org/10.1016/j.jmrt.2021.07.082
18. Hutsaylyuk V., Student M., Posuvailo V., Student O., Sirak Y., Hvozdets'kyi V., Maruschak P., Veselivska H., The properties of oxide-ceramic layers with Cu and Ni inclusions synthesizing by PEO method on top of the gas-spraying coatings on aluminium alloys, Vacuum, 2020; 179: 109514, https://doi.org/10.1016/j.vacuum.2020.109514
19. O'Brien T.E., Chaklader A.C.D. Effect of oxygen on the reaction between copper and sapphire. Journal of the American Ceramic Society 1974; 57: 329–332. https://doi.org/10.1111/j.1151-2916.1974.tb10915.x
20. Yoshino Y. Role of oxygen in bonding copper to alumina. Journal of the American Ceramic Society 1989; 72: 1322–1327. https://doi.org/10.1111/j.1151-2916.1989.tb07645.x
21. Diemer M.W., Neubrand A., Trumble K.P., Rödel J. Influence of oxygen partial pressure and oxygen content on the wettability in the copper–oxygen–alumina system. Journal of the American Ceramic Society 2004; 82: 2825–2832. https://doi.org/10.1111/j.1151-2916.1999.tb02163.x
22. Wang S.W., Chen L.D., Hirai T. Densification of Al_2O_3 powder using spark plasma sintering. Journal of Materials Research 2000; 15: 982–987. https://doi.org/10.1557/JMR.2000.0140
23. Guo X., Xu G., Li S., Song K., Liu S., Wang X., Luo Q., Liu H., Song H. Enhanced plastic deformation ability of copper matrix composites through synergistic strengthening of nano- Al_2O_3 and Cr particles. Materials Science and Engineering A 2024; 910: 146886. https://doi.org/10.1016/j.msea.2024.146886
24. Ding X.-Y., Fu Y.-C., Li B., Lin S., Luo L.-M., Wu Y.-C., Yao J.-H. Microstructure and mechanical properties of Al_2O_3 dispersion strengthened Cu by laser in-situ aluminum thermal reduction processing. Materials & Design 2025; 258: 114547. https://doi.org/10.1016/j.matdes.2025.114547
25. Piotrkiewicz P., Zygmuntowicz J., Wachowski M., Cymerman K., Kaszuwara W., Więcław-Midor A. Al_2O_3-Cu-Ni composites manufactured via uniaxial pressing: Microstructure, magnetic, and mechanical properties. Materials 2022; 15(5): 1848. https://doi.org/10.3390/ma15051848
26. Zygmuntowicz J., Falkowski P., Miazga A., Konopka K. Fabrication and characterization of ZrO_2/Ni composites. Journal of the Australian Ceramic Society 2018; 54(4): 655–662. https://doi.org/10.1007/s41779-018-0194-3
27. Lis J., Pampuch R. Spiekanie. Kraków: AGH Uczelniane Wydawnictwa Naukowo-Dydaktyczne; 2000.
28. Gizowska M., Miazga A., Konopka K., Szafran M. The influence of sintering temperature on properties of Al_2O_3-Ni composites. Composites Theory and Practice 2012; 12(1): 33–38.
29. PN-EN ISO 18754:2022-10. Ceramika wysokiej jakości – oznaczanie gęstości i porowatości otwartej.
30. Lankford J. Indentation microfracture in the Palmqvist crack regime: Implications for fracture toughness evaluation by the indentation method. Journal of Materials Science Letters 1982; 1(11): 493–495. https://doi.org/10.1007/BF00721938
31. SpychalskiW.L., Kurzydłowski K.J. and Ralph B. (2002). Computer study of inter- and intragranular surface cracks in brittle polycrystals, Materials Characterization 49(9): 45–53.
32. Wejrzanowski T., Kurzydłowski K.J. Stereology of grains in nanocrystals. Solid State Phenomena 2003; 94: 221–228. https://doi.org/10.4028/www.scientific.net/SSP.94.221
33. Wejrzanowski T., Spychalski W., Rożniatowski K., Kurzydłowski K. Image-based analysis of complex microstructures of engineering materials. International Journal of Applied Mathematics and Computer Science 2008; 18(1): 33–39. https://doi.org/10.2478/v10006-008-0003-1
34. Michalski J., Wejrzanowski T., Pielaszek R., Konopka K., Łojkowski W., Kurzydłowski K.J. Application of image analysis for characterization of powders. Materials Science Poland 2005; 23: 79–86.
35. Ryś J. Stereologia materiałów. Kraków: Fotobit-Design; 1995.
36. Shackelford J.F., Han Y.H., Kim S., Kwon S.H. CRC materials science and engineering handbook.

CRC Press; 2016. https://doi.org/10.1201/b18971

37. Konopka K., Zygmuntowicz J., Krasnowski M., Cymerman K., Wachowski M., Piotrkiewicz P. Pulse plasma sintering of NiAl- Al_2O_3 composite powder produced by mechanical alloying with contribution of nanometric Al_2O_3 powder. Materials 2022; 15(2): 407. https://doi.org/10.3390/ma15020407
38. Huang S., Vanmeensel K., Van der Biest O., Vleugels J. Pulsed electric current sintering and characterization of ultrafine Al2O3–WC composites. Materials Science and Engineering A 2010; 527(3): 584–589. https://doi.org/10.1016/j.msea.2009.08.035
39. Gross T.M., Liu H., Zhai Y., Huang L., Wu J. The impact of densification on indentation fracture toughness measurements. Journal of the American Ceramic Society 2020; 103(7): 3920–3929. https://doi.org/10.1111/jace.16793
40. Feng Y., Zhang T. Determination of fracture toughness of brittle materials by indentation. Acta Mechanica Solida Sinica 2015; 28(3): 221–234. https://doi.org/10.1016/S0894-9166(15)30010-0
41. Solomah A.G. Indentation techniques in ceramic materials characterization: Theory and practice. John Wiley & Sons; 2012.